Heralded quantum gates for hybrid systems via waveguide-mediated photon scattering

Guo-Zhu Song,[1,*] Jin-Liang Guo,[1] Qian Liu,[2] Hai-Rui Wei,[3] and Gui-Lu Long[4,5,6,7]

[1]*College of Physics and Materials Science, Tianjin Normal University, Tianjin 300387, China*
[2]*School of Science, Qingdao University of Technology, Qingdao 266520, China*
[3]*School of Mathematics and Physics, University of Science and Technology Beijing, Beijing 100083, China*
[4]*State Key Laboratory of Low-Dimensional Quantum Physics and Department of Physics, Tsinghua University, Beijing 100084, China*
[5]*Beijing National Research Center for Information Science and Technology, Beijing 100084, China*
[6]*Frontier Science Center for Quantum Information, Beijing 100084, China*
[7]*Beijing Academy of Quantum Information Sciences, Beijing 100193, China*

(Received 5 January 2021; accepted 8 July 2021; published 20 July 2021)

Universal quantum gates play a critical role in quantum information processing. Here, based on the scattering property of photons off single emitters in one-dimensional waveguides, we present some heralded protocols for realizing controlled-NOT, Toffoli, and Fredkin gates on hybrid systems. The control qubit of our gates is encoded on a flying photon, and the target qubits are encoded in the degenerate ground states of the emitter. In our schemes, the faulty scattering processes between emitters and photons caused by system imperfections can be transformed into the detection of photon polarization. That is, our three quantum gates are accomplished in a heralded way. Moreover, the quantum circuits for the three gates are versatile and compact, and no additional qubits are required. With current technique on manipulating the emitter-waveguide system, our protocols may be experimentally feasible. This work provides an effective avenue for implementing quantum logic gates.

DOI: 10.1103/PhysRevA.104.012608

I. INTRODUCTION

Quantum logic gates are the building blocks of quantum circuits, which are essential for quantum computation and quantum information processing [1]. It has been shown that any unitary operation can be realized by using only single qubit gates and the controlled-not (CNOT) gate [2,3]. The CNOT gate is the most important two qubit gate and has attracted much attention in the past decades [4–13]. Even though CNOT gates together with single qubit operations are sufficient for universal quantum computation, the performance of quantum circuits can be improved by using three-qubit quantum gates including Toffoli and Fredkin gates [14]. Moreover, universal quantum gates are also vital elements in the implementation of quantum algorithms, such as the best-known Shor algorithm [15] and Grover/Long algorithm [16,17], phase estimation algorithm [18], and so on.

In the past decades, many approaches for quantum logic gates have been presented in various physical systems, such as quantum dots [19–24], superconducting qubits [25–30], nuclear magnetic resonance [31–34], diamond nitrogen-vacancy center [35–38], and so on. In 2010, based on the interface between a photon and an electron confined in a quantum dot embedded in a microcavity, Bonato *et al.* constructed a spin-photon CNOT gate [39]. Later, Fedorov *et al.* realized a Toffoli gate with three superconducting transmon qubits dispersively coupled to a microwave resonator [40]. By exploiting path-mode entanglement to add control to the SWAP operation, Patel *et al.* utilized linear optics to implement a demonstration of the Fredkin gate [41]. Recently, Liu and Wei presented two compact protocols for realizing a three-qubit deterministic Fredkin gate and a non-deterministic Fredkin gate in a multilevel system [42].

Different from the above important schemes for quantum gates, we here focus on the realization of robust-fidelity photon-emitter hybrid gates in one-dimensional (1D) waveguides. The waveguide platforms include various nanophotonic structures such as optical nanofibers [43–50], plasmonic nanowires [51,52], photonic crystal waveguides [53–56], diamond-based waveguides [57–59], or superconducting transmission lines [60–64]. Especially, a two-level quantum emitter with ground state $|g\rangle$ and excited state $|e\rangle$ coupled to electromagnetic modes of a 1D waveguide has been studied [65,66]. Ideally, due to quantum interference, a photon with frequency resonant to the two-level emitter can be perfectly reflected, i.e., the quantum emitter can behave as a photon mirror. Besides, an Λ-type three-level emitter is also considered [52], where the states $|g\rangle$ and $|e\rangle$ remain coupled via waveguide modes and the extra metastable level is decoupled from waveguide modes. It is found that a single-photon transistor can be created by combining the state-dependent conditional reflection and single-photon storage. Moreover, Li *et al.* studied the scattering property a four-level emitter with degenerate ground and excited states coupled to a 1D waveguide and constructed a robust-fidelity atom-photon entangling gate [67]. In their scheme, the physical errors arising from imperfections of the atom-waveguide system can be heralded by detecting the polarization state of the output photon. Recently, great progress has been made in waveguide-QED

*Corresponding author: songguozhu@tjnu.edu.cn

platforms, which paves the way to its applications in quantum information processing and quantum network [68–82].

In this paper, by utilizing the scattering principle of photons off single emitters in the 1D waveguide, we propose some heralded schemes for realizing CNOT, Toffoli, and Fredkin gates on photon-emitter hybrid systems. The control qubit of the gates in our proposal is encoded on a flying photon, i.e., the two polarization states of a single photon, and the target qubits are encoded in the degenerate ground states of the emitter coupled to 1D waveguides. In our schemes, the imperfect scattering processes between emitters and photons in 1D waveguides, caused by frequency detunings, weak couplings, and finite bandwidths of the incident photonic pulses, can be transformed into the detection of photon polarization. In other words, the faulty events in our protocols can be alarmed by the single-photon detector, i.e., our three quantum gates are accomplished in a heralded way. Moreover, the protocols for the three quantum gates are compact and versatile, and any auxiliary qubits are not needed. With remarkable advances to interface quantum emitters with nanophotonic waveguide [83–85], these unique features make our schemes highly advantageous to realize feasible quantum information processing.

The paper is organized as follows: In Sec. II, the transport property of a photon scattering with a two-level emitter coupled to a 1D waveguide is introduced. In Sec. III, we present a heralded scheme for implementing a CNOT gate on a two-qubit hybrid system. Subsequently, the quantum circuits for constructing three-qubit Toffoli and Fredkin gates on photon-emitter hybrid systems are given in Secs. IV and V, respectively. Finally, a discussion about the feasibility of our schemes with current experimental technology and a summary are shown in Sec. VI.

II. THE SCATTERING OF PHOTONS OFF SINGLE EMITTERS

As shown in Fig. 1(a), we consider a system composed of a two-level emitter coupled to electromagnetic modes in a 1D waveguide. The emitter has two electronic levels, i.e., the ground state $|g\rangle$ and the excited state $|e\rangle$ with frequency difference ω_0. Assuming that the resonance frequency ω_0 is away from the cutoff frequency of the waveguide, we can write the Hamiltonian of the system in real space as ($\hbar = 1$) [52,65]

$$H=\left(\omega_0-\frac{i\gamma_e'}{2}\right)\sigma_{ee}+iv_g\int dz\left[c_L^\dagger(z)\frac{\partial c_L(z)}{\partial z}-c_R^\dagger(z)\frac{\partial c_R(z)}{\partial z}\right]$$
$$+V\int dz\delta(z)\{\sigma_{eg}[c_R(z)+c_L(z)]+\text{H.c.}\}, \quad (1)$$

where γ_e' is the decay rate of the state $|e\rangle$ into free space, v_g is the group velocity of photons, and c_L (c_R) represents the annihilation operator of the left (right) propagating field. V is the coupling strength between the emitter and the waveguide modes, assumed to be identical for all modes. The emitter operator $\sigma_{\alpha\beta}=|\alpha\rangle\langle\beta|$, where $\alpha,\beta=g,e$.

Provided that a single-photon wave packet with energy $E_k=v_gk$ is coming in from the left (k denotes the wave vector of the photon), and the emitter is initially at the ground state $|g\rangle$. The general state of the photon-emitter system takes the following form:

$$|\Psi_k\rangle=\int dz[\psi_{k,L}(z)c_L^\dagger(z)+\psi_{k,R}(z)c_R^\dagger(z)]|\text{vac},g\rangle$$
$$+e_k|\text{vac},e\rangle, \quad (2)$$

where $\psi_{k,L}(z)$ and $\psi_{k,R}(z)$ represent the probability amplitudes of the left- and right-propagating photons at position z, respectively. $|\text{vac}\rangle$ indicates the vacuum state containing zero photon and e_k is the probability amplitude of the emitter in the excited state. Since the photon is incident from the left, $\psi_{k,L}(z)$ and $\psi_{k,R}(z)$ take the forms:

$$\psi_{k,L}(z)=re^{-ikz}\theta(-z),$$
$$\psi_{k,R}(z)=e^{ikz}\theta(-z)+te^{ikz}\theta(z), \quad (3)$$

where r and t denote the reflection and transmission amplitudes, respectively. $\theta(z)$ is Heaviside step function.

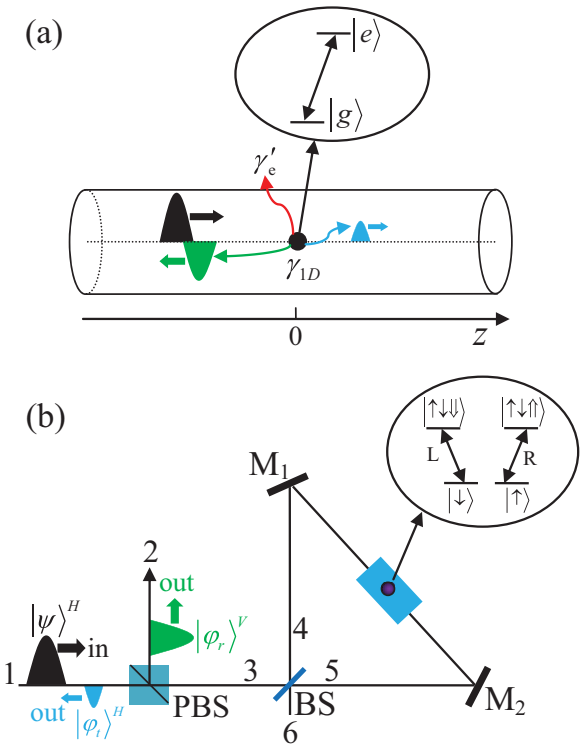

FIG. 1. (a) Schematic diagram for a photon mirror where a two-level emitter (the black dot) is coupled to a 1D waveguide (the cylinder). An input photon (black wave packet) from the left interacts with the emitter, which generates a transmitted component (blue wave packet) and a reflected component (green wave packet). (b) A heralded protocol for realizing a Z gate on an emitter confined in a 1D waveguide. PBS represents a polarizing beam splitter, which reflects the photon in the vertical polarization state $|V\rangle$ and transmits the photon in the horizontal polarization state $|H\rangle$. *BS* is a 50:50 beam splitter, M_i ($i=1,2$) is a fully reflected mirror, and the black lines denote free space photon paths. The inset shows four-level structure and optical transitions of a negatively charged quantum dot, i.e., the emitter. The ground state $|\uparrow\rangle$ ($|\downarrow\rangle$) is the electron-spin state with $J_z=\frac{1}{2}$ ($J_z=-\frac{1}{2}$); $|\uparrow\downarrow\Uparrow\rangle$ ($|\uparrow\downarrow\Downarrow\rangle$) denotes the trion state of a negatively charged exciton with $J_z=\frac{3}{2}$ ($J_z=-\frac{3}{2}$).

By solving the scattering eigenvalue equation $H|\Psi_k\rangle = E_k|\Psi_k\rangle$, we can get the reflection amplitude r for the input photon as [52,65]

$$r = -\frac{1}{1 + 1/P - 2i\Delta/\gamma_{1D}}, \tag{4}$$

where $P = \gamma_{1D}/\gamma_e'$ is the Purcell factor with $\gamma_{1D} = 4\pi V^2/v_g$ being the rate of emitter decay into the waveguide modes. $\Delta = \omega_{in} - \omega_0$ is the frequency detuning between the input photon and the emitter transition. The transmission amplitude t is given by $t = 1 + r$. From Eq. (4), we can find that the reflection amplitude turns to be $r \approx -1$ when the incident photon resonates with the emitter ($\Delta = 0$) and the Purcell factor P is sufficiently large. That is, in such a case, the emitter acts as a photon mirror, which puts a π-phase shift on the reflected part of the photon [65]. While, when the emitter is decoupled from the waveguide modes, the incident photon transmits through the emitter with no effect.

In the following, we consider a four-level emitter coupled to a 1D waveguide, as shown in Fig. 1(b). Such an emitter can be realized by a singly charged self-assembled InGaAs/GaAs quantum dot [86,87]. The optical transition $|\downarrow\rangle \leftrightarrow |\uparrow\downarrow\Downarrow\rangle$ ($|\uparrow\rangle \leftrightarrow |\uparrow\downarrow\Uparrow\rangle$) is driven by the absorption or emission of a left-circularly (right-circularly) polarized photon $|L\rangle$ ($|R\rangle$). For simplicity, in the following presentation, we write the above states as: $|\downarrow\rangle = |g_-\rangle$, $|\uparrow\rangle = |g_+\rangle$. Assuming that the spatial wave function of the incident photon from left is $|\psi\rangle$, with the scattering principle mentioned above, we can get

$$\begin{aligned}
|g_-\rangle|\psi\rangle|L\rangle &\rightarrow |g_-\rangle|\phi\rangle|L\rangle,\\
|g_-\rangle|\psi\rangle|R\rangle &\rightarrow |g_-\rangle|\psi\rangle|R\rangle,\\
|g_+\rangle|\psi\rangle|R\rangle &\rightarrow |g_+\rangle|\phi\rangle|R\rangle,\\
|g_+\rangle|\psi\rangle|L\rangle &\rightarrow |g_+\rangle|\psi\rangle|L\rangle.
\end{aligned} \tag{5}$$

Here, $|\phi\rangle = |\phi_r\rangle + |\phi_t\rangle$ is the photon component in the waveguide after the scattering process. $|\phi_r\rangle = r|\psi\rangle$ and $|\phi_t\rangle = t|\psi\rangle$ are the spatial wave functions of the reflected and transmitted parts of the photon, respectively. Provided that the incident photon is initially prepared in the horizontal linear-polarization state $|H\rangle = (|R\rangle + |L\rangle)/\sqrt{2}$, the hybrid system consisting of the single photon and the emitter evolves as follows:

$$\begin{aligned}
|g_-\rangle|\psi\rangle|H\rangle &\rightarrow \tfrac{1}{2}|g_-\rangle[(|\phi\rangle + |\psi\rangle)|H\rangle - (|\phi\rangle - |\psi\rangle)|V\rangle],\\
|g_+\rangle|\psi\rangle|H\rangle &\rightarrow \tfrac{1}{2}|g_+\rangle[(|\phi\rangle + |\psi\rangle)|H\rangle + (|\phi\rangle - |\psi\rangle)|V\rangle],
\end{aligned} \tag{6}$$

where $|V\rangle = (|R\rangle - |L\rangle)/\sqrt{2}$ is the vertical linear-polarization state. In fact, due to the relation $t = 1 + r$, we easily obtain $(|\phi\rangle + |\psi\rangle)/2 = |\phi_t\rangle$ and $(|\phi\rangle - |\psi\rangle)/2 = |\phi_r\rangle$. Thus, the transformations in Eq. (6) are changed into

$$\begin{aligned}
|g_-\rangle|\psi\rangle|H\rangle &\rightarrow |g_-\rangle|\phi_t\rangle|H\rangle - |g_-\rangle|\phi_r\rangle|V\rangle,\\
|g_+\rangle|\psi\rangle|H\rangle &\rightarrow |g_+\rangle|\phi_t\rangle|H\rangle + |g_+\rangle|\phi_r\rangle|V\rangle.
\end{aligned} \tag{7}$$

Interestingly, when the incident photon is in the state $|H\rangle$, after the scattering process, the output photon contains the components in states $|H\rangle$ and $|V\rangle$ simultaneously. In particular, when the emitter is initially in the state $|g_-\rangle$, a π-phase shift occurs on the emitter for the photon component $|V\rangle$.

Assisted by the single-photon input-output process, a heralded Z gate on an emitter confined in a 1D waveguide can be realized, as shown in Fig. 1(b). In detail, suppose that a photon in spatial state $|\psi\rangle$ and polarization state $|H\rangle$ is injected into the setup from port 1. First, it transmits through a polarizing beam splitter (PBS) and arrives at port 3. Then, it is split by a 50:50 beam splitter (*BS*), and the reflected photon component in path 4 and transmitted photon component in path 5 scatter with the emitter independently. After the scattering processes, the two parts of the photon in paths 4 and 5 travel back and interfere with each other at the *BS*, and quit the device from port 3. Finally, the photon wave packet goes through PBS, and the photon part in state $|H\rangle$ ($|V\rangle$) exits from port 1 (2). The above processes can be described as follows [67]:

$$\begin{aligned}
|\Phi_0\rangle &= |g_\pm\rangle|\psi\rangle|H\rangle^1\\
&\xrightarrow{\text{PBS}} |g_\pm\rangle|\psi\rangle|H\rangle^3\\
&\xrightarrow{\text{BS}} \frac{1}{\sqrt{2}}|g_\pm\rangle|\psi\rangle|H\rangle^4 + \frac{1}{\sqrt{2}}|g_\pm\rangle|\psi\rangle|H\rangle^5\\
&\xrightarrow{\text{Scatter}} \frac{1}{\sqrt{2}}|g_\pm\rangle|\phi_t\rangle|H\rangle^4 + \frac{1}{\sqrt{2}}|g_\pm\rangle|\phi_t\rangle|H\rangle^5\\
&\quad \pm\frac{1}{\sqrt{2}}|g_\pm\rangle|\phi_r\rangle|V\rangle^4 \pm \frac{1}{\sqrt{2}}|g_\pm\rangle|\phi_r\rangle|V\rangle^5\\
&\xrightarrow{\text{BS}} |g_\pm\rangle|\phi_t\rangle|H\rangle^1 \pm |g_\pm\rangle|\phi_r\rangle|V\rangle^2,
\end{aligned} \tag{8}$$

where the superscripts $1, 2, 3, 4, 5$ denote the paths of the photon shown in Fig. 1(b). In fact, with the polarization filtering of PBS, the horizontal polarization output in Eq. (8) can be discarded. Thus, when the incident photon is initially in the state $|H\rangle$, the evolutions of the scattering setup can be described as follows:

$$\begin{aligned}
|g_-\rangle|\psi\rangle|H\rangle &\rightarrow -|g_-\rangle|\phi_r\rangle|V\rangle,\\
|g_+\rangle|\psi\rangle|H\rangle &\rightarrow +|g_+\rangle|\phi_r\rangle|V\rangle.
\end{aligned} \tag{9}$$

Similarly, suppose that the input photon (from port 2) is in the vertical linear-polarization state $|V\rangle$, discarding the photon output with unchanged polarization state, we can obtain the corresponding evolutions:

$$\begin{aligned}
|g_-\rangle|\psi\rangle|V\rangle &\rightarrow -|g_-\rangle|\phi_r\rangle|H\rangle,\\
|g_+\rangle|\psi\rangle|V\rangle &\rightarrow +|g_+\rangle|\phi_r\rangle|H\rangle.
\end{aligned} \tag{10}$$

Note that, due to the destructive quantum interference, no photon component exits from port 6 though faulty scattering event occurs in the device. As we mention above, $|\phi_r\rangle$ is the spatial state of the reflected photon component. For a perfect scattering process, i.e., $P \rightarrow \infty$ and $\Delta = 0$, $|\phi_r\rangle = -|\psi\rangle$. While, in a practical emitter-waveguide system, P is finite and $|\phi_r\rangle \neq -|\psi\rangle$. In this case, the faulty event corresponds to the photon output with unchanged polarization state, which can be discarded. In other words, the device for realizing Z gate shown in Fig. 1(b) works in a heralded manner. For a realistic quantum dot in experiment, due to the heavy-light hole mixing, the optical selection rule is imperfect, i.e., the cross transitions in Fig. 1(b) are weakly allowed through the

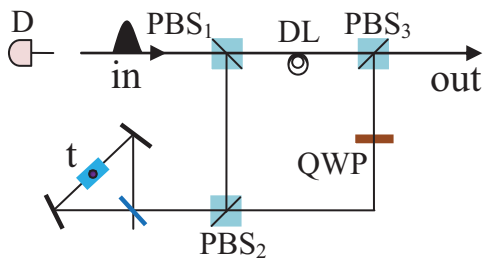

FIG. 2. Quantum circuit for constructing a CNOT gate with a flying photon as the control qubit and an emitter confined in the 1D waveguide as the target qubit. D denotes a single-photon detector, and QWP represents a quarter-wave plate to realize the conversion of the photon polarization. DL is a time-delay device which makes the two wave packets emitting from PBS_1 and QWP reach PBS_3 simultaneously.

light-hole component of the hole spin states [87]. Fortunately, this hole mixing can be reduced by choosing the appropriate types of quantum dots and engineering the direction of the external magnetic field, and in the valence band is on the order of a few percent [88]. Thus, this can reduce the scattering fidelity by only a few percent. In the following sections, based on the scattering principles, i.e., Eqs. (9) and (10), we present heralded schemes for constructing CNOT, Toffoli, and Fredkin gates on photon-emitter hybrid systems.

III. CNOT GATE ON A TWO-QUBIT HYBRID SYSTEM

A CNOT gate on a two-qubit bybrid system is used to flip the target qubit if the control photon qubit is in the state $|V\rangle$; otherwise, the state of the target qubit does not change. The schematic diagram for our CNOT gate is depicted in Fig. 2. We describe its principle in detail as follows.

Suppose that the flying photon p and the emitter t trapped in the 1D waveguide are prepared in arbitrary superposition polarizations states $|\varphi\rangle_p = \alpha_p|H\rangle + \beta_p|V\rangle$ and $|\varphi\rangle_t = \alpha|0\rangle + \beta|1\rangle$, respectively. Here the unknown coefficients satisfy $|\alpha_p|^2 + |\beta_p|^2 = |\alpha|^2 + |\beta|^2 = 1$, and $|0\rangle = |g_-\rangle$, $|1\rangle = |g_+\rangle$. First, the input photon with spatial wave function $|\psi\rangle$ passes through PBS_1, which reflects the photon in state $|V\rangle$ and transmits the photon in state $|H\rangle$. That is, the photon in state $|V\rangle$ is reflected by PBS_1 and arrives at PBS_2, while the photon in state $|H\rangle$ transmits through PBS_1 and arrives at PBS_3. After the above processes, the state of the hybrid system is

$$|\Psi_0\rangle = \alpha_p|\psi\rangle|H\rangle(\alpha|0\rangle+\beta|1\rangle)+\beta_p|\psi\rangle|V\rangle(\alpha|0\rangle+\beta|1\rangle). \quad (11)$$

Second, the photon in state $|V\rangle$ is reflected by PBS_2 into the scattering configuration to interact with emitter t. Before this interaction, a Hadamard operation (e.g., using a $\pi/2$ microwave pulse or optical pulse [89,90]) is performed on emitter t complete the transformations $|0\rangle \to \frac{1}{\sqrt{2}}(|0\rangle + |1\rangle)$ and $|1\rangle \to \frac{1}{\sqrt{2}}(|0\rangle - |1\rangle)$. Thus, the state of the whole system becomes

$$|\Psi_1\rangle = \frac{1}{\sqrt{2}}\{\alpha_p|\psi\rangle|H\rangle[\alpha(|0\rangle + |1\rangle) + \beta(|0\rangle - |1\rangle)] + \beta_p|\psi\rangle|V\rangle[\alpha(|0\rangle + |1\rangle) + \beta(|0\rangle - |1\rangle)]\}. \quad (12)$$

Third, the photon in state $|V\rangle$ interacts with the emitter t confined in the 1D waveguide and the state of the hybrid system evolves into

$$|\Psi_2\rangle = \frac{1}{\sqrt{2}}\{\alpha_p|\psi\rangle|H\rangle[\alpha(|0\rangle + |1\rangle) + \beta(|0\rangle - |1\rangle)] - \beta_p r|\psi\rangle|H\rangle[\alpha(|0\rangle - |1\rangle) + \beta(|0\rangle + |1\rangle)]\}, \quad (13)$$

where r is the reflection amplitude of the input field mentioned above. After the interaction between the photon and the emitter t confined in the 1D waveguide, a Hadamard operation is also performed on the emitter t, i.e., $|0\rangle \to \frac{1}{\sqrt{2}}(|0\rangle + |1\rangle)$ and $|1\rangle \to \frac{1}{\sqrt{2}}(|0\rangle - |1\rangle)$. Thus, the state of the hybrid system becomes

$$|\Psi_3\rangle = \alpha_p|\psi\rangle|H\rangle(\alpha|0\rangle+\beta|1\rangle)-\beta_p r|\psi\rangle|H\rangle(\alpha|1\rangle+\beta|0\rangle). \quad (14)$$

Then, the photon part coming from the scattering device transmits through PBS_2 and a quarter-wave plate (QWP) successively. Finally, this photon part and another photon part coming directly from PBS_1 through the time-delay device (DL) simultaneously arrive at PBS_3 and interfere with each other. After above processes, the state of the system is transformed into

$$|\Psi_4\rangle = \alpha_p|\psi\rangle|H\rangle(\alpha|0\rangle+\beta|1\rangle)-\beta_p r|\psi\rangle|V\rangle(\alpha|1\rangle+\beta|0\rangle). \quad (15)$$

For a perfect scattering process, i.e., $r = -1$, the above state becomes

$$|\Psi_5\rangle = \alpha_p|\psi\rangle|H\rangle(\alpha|0\rangle+\beta|1\rangle)+\beta_p|\psi\rangle|V\rangle(\alpha|1\rangle+\beta|0\rangle). \quad (16)$$

From Eq. (16), one can see that the device shown in Fig. 2 implements a CNOT gate for the hybrid system, which flips the state of the target qubit when the photon (the control qubit) is in the state $|V\rangle$; otherwise, nothing is done on the emitter.

In fact, our protocol for realizing a CNOT gate is accomplished in a heralded way. That is, if the detector D clicks, it indicates that faulty interaction (no scattering event) between the flying photon and emitter t happens. In such a case, the state of the target qubit is not changed. Thus, we need not reinitialize the target qubit when we input another photon into the device to realize the CNOT gate again. As mentioned in Sec. II, the four-level emitter can be realized by a singly charged self-assembled InGaAs/GaAs quantum dot. Thus, single photons needed in our setup can be experimentally generated by single-photon sources based on quantum dots [91,92]. With a single photon, e.g., $|H\rangle$, one can obtain an arbitrary state of the photonic qubit (i.e., $\alpha_p|H\rangle + \beta_p|V\rangle$) with a QWP-HWP-QWP sequence [93], where QWP and HWP denote a quarter-wave plate and a half-wave plate, respectively.

IV. TOFFOLI GATE ON A THREE-QUBIT HYBRID SYSTEM

A Toffoli gate on a hybrid system is used to flip the state of the target qubit when the control photon qubit is in the state $|V\rangle$ and the control qubit is in the state $|1\rangle$; otherwise, nothing is done on the target qubit. Our device for realizing a Toffoli gate on a flying photon and two emitters is shown in Fig. 3. The principle of this Toffoli gate is given in detail as follows.

Assume that the control photon qubit p with spatial wave function $|\psi\rangle$ is initially prepared in an arbitrary superposition

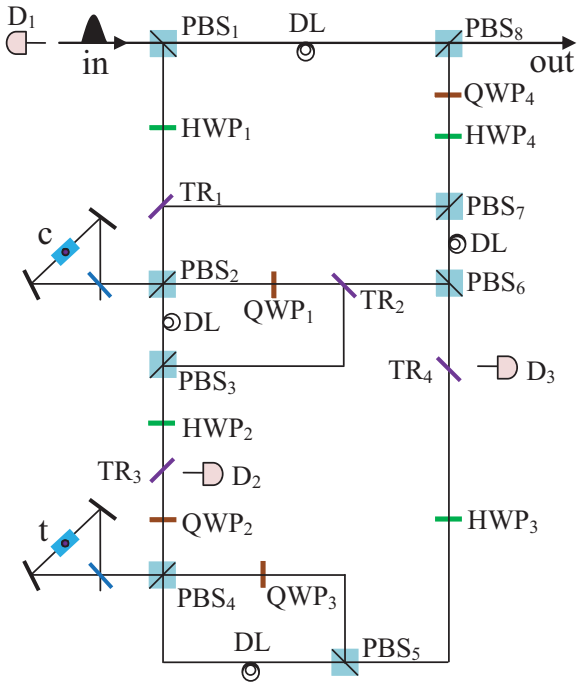

FIG. 3. Schematic diagram for realizing a three-qubit Toffoli gate with a flying photon and an emitter confined in the 1D waveguide as the two control qubits and another confined emitter as the target qubit. HWP represents a half-wave plate to perform a Hadamard operation on the photon. TR denotes an optical switch, which can be controlled exactly as needed to reflect or transmit a photon. In experiment, an optical switch can be well realized by an electro-optic modulator [94,95].

polarizations state $|\varphi\rangle_p = \alpha_p|H\rangle + \beta_p|V\rangle$, and the control qubit c and the target qubit t are originally prepared in arbitrary states $|\varphi\rangle_c = \alpha_c|0\rangle + \beta_c|1\rangle$ and $|\varphi\rangle_t = \alpha_t|0\rangle + \beta_t|1\rangle$, respectively. Here,

$$|\alpha_p|^2 + |\beta_p|^2 = |\alpha_c|^2 + |\beta_c|^2 = |\alpha_t|^2 + |\beta_t|^2 = 1. \quad (17)$$

We first inject the photon from the port *in* and it passes through PBS_1, which reflects the photon in state $|V\rangle$ and transmits the photon in state $|H\rangle$. The photon in state $|H\rangle$ goes through PBS_1 and arrives at PBS_8, while the part in state $|V\rangle$ is reflected by PBS_1 and travels through a half-wave plate (HWP_1) and an optical switch (TR_1)(transmit). After above processes, the state of the whole system is changed from $|\Phi_0\rangle = |\psi\rangle|\varphi\rangle_p \otimes |\varphi\rangle_c \otimes |\varphi\rangle_t$ to $|\Phi_1\rangle$, where

$$\begin{aligned}|\Phi_1\rangle = {} & \alpha_p|\psi\rangle|H\rangle(\alpha_c|0\rangle+\beta_c|1\rangle)_c(\alpha_t|0\rangle+\beta_t|1\rangle)_t \\ & + \frac{\beta_p}{\sqrt{2}}|\psi\rangle(|H\rangle-|V\rangle)(\alpha_c|0\rangle+\beta_c|1\rangle)_c(\alpha_t|0\rangle+\beta_t|1\rangle)_t.\end{aligned} \quad (18)$$

Second, the photon goes through PBS_2 and is split into two wave packets. In detail, the part in state $|V\rangle$ is reflected by PBS_2 to interact with the control qubit c, while the part in state $|H\rangle$ transmits through PBS_2 and arrives at PBS_3. Then, getting out from the scattering setup containing emitter c, the former photon part passes through PBS_2 and QWP_1, and is reflected by TR_2 to interfere with the latter photon part in PBS_3. After PBS_3, the state of the whole system collapses into $|\Phi_2\rangle$, where

$$\begin{aligned}|\Phi_2\rangle = {} & \alpha_p|\psi\rangle|H\rangle(\alpha_c|0\rangle+\beta_c|1\rangle)_c(\alpha_t|0\rangle+\beta_t|1\rangle)_t \\ & + \frac{\beta_p}{\sqrt{2}}|\psi\rangle|H\rangle(\alpha_c|0\rangle+\beta_c|1\rangle)_c(\alpha_t|0\rangle+\beta_t|1\rangle)_t \\ & + \frac{\beta_p r}{\sqrt{2}}|\psi\rangle|V\rangle(\alpha_c|0\rangle-\beta_c|1\rangle)_c(\alpha_t|0\rangle+\beta_t|1\rangle)_t. \quad (19)\end{aligned}$$

Third, the photon part coming from PBS_3 travels through HWP_2, TR_3 (transmit) and QWP_2, and is split by PBS_4 into two parts. The part in state $|H\rangle$ passes through PBS_4 and arrives at PBS_5 directly. The other part in state $|V\rangle$ interacts with the target qubit t, and goes through PBS_4 and QWP_3. Note that, before and after the interaction between the photon and the target qubit t, a Hadamard operation is performed on emitter t. The two parts of the photon get together at PBS_5. After that, the state of the system evolves into

$$\begin{aligned}|\Phi_3\rangle = {} & \alpha_p|\psi\rangle|H\rangle(\alpha_c|0\rangle+\beta_c|1\rangle)_c(\alpha_t|0\rangle+\beta_t|1\rangle)_t \\ & + \frac{(1-r)\beta_p}{2}|\psi\rangle|H\rangle(\alpha_c\alpha_t|0\rangle_c|0\rangle_t + \alpha_c\beta_t|0\rangle_c|1\rangle_t) \\ & + \frac{(1+r)\beta_p}{2}|\psi\rangle|H\rangle(\beta_c\alpha_t|1\rangle_c|0\rangle_t + \beta_c\beta_t|1\rangle_c|1\rangle_t) \\ & - \frac{(1+r)r\beta_p}{2}|\psi\rangle|V\rangle(\alpha_c\alpha_t|0\rangle_c|1\rangle_t + \alpha_c\beta_t|0\rangle_c|0\rangle_t) \\ & - \frac{(1-r)r\beta_p}{2}|\psi\rangle|V\rangle(\beta_c\alpha_t|1\rangle_c|1\rangle_t + \beta_c\beta_t|1\rangle_c|0\rangle_t).\end{aligned} \quad (20)$$

Fourth, the photon passes through HWP_3 and TR_4 (transmit), and is split by PBS_6 into two parts. The part in the state $|H\rangle$ passes through PBS_6 and arrives at PBS_7 directly. While, the part in the state $|V\rangle$ experiences a series of operations as follows: $PBS_6 \rightarrow TR_2$ (transmit) $\rightarrow QWP_1 \rightarrow PBS_2 \rightarrow$ emitter $c \rightarrow PBS_2 \rightarrow TR_1$ (reflect) $\rightarrow PBS_7$. After the two parts get together at PBS_7, the state of the whole system becomes

$$\begin{aligned}|\Phi_4\rangle = {} & \alpha_p|\psi\rangle|H\rangle(\alpha_c|0\rangle+\beta_c|1\rangle)_c(\alpha_t|0\rangle+\beta_t|1\rangle)_t \\ & + \frac{(1-r)\beta_p}{2\sqrt{2}}|\psi\rangle|H\rangle(\alpha_c\alpha_t|0\rangle_c|0\rangle_t + \alpha_c\beta_t|0\rangle_c|1\rangle_t) \\ & + \frac{(1+r)\beta_p}{2\sqrt{2}}|\psi\rangle|H\rangle(\beta_c\alpha_t|1\rangle_c|0\rangle_t + \beta_c\beta_t|1\rangle_c|1\rangle_t) \\ & - \frac{(1+r)r\beta_p}{2\sqrt{2}}|\psi\rangle|H\rangle(\alpha_c\alpha_t|0\rangle_c|1\rangle_t + \alpha_c\beta_t|0\rangle_c|0\rangle_t) \\ & - \frac{(1-r)r\beta_p}{2\sqrt{2}}|\psi\rangle|H\rangle(\beta_c\alpha_t|1\rangle_c|1\rangle_t + \beta_c\beta_t|1\rangle_c|0\rangle_t) \\ & - \frac{(1-r)r\beta_p}{2\sqrt{2}}|\psi\rangle|V\rangle(\alpha_c\alpha_t|0\rangle_c|0\rangle_t + \alpha_c\beta_t|0\rangle_c|1\rangle_t) \\ & + \frac{(1+r)r\beta_p}{2\sqrt{2}}|\psi\rangle|V\rangle(\beta_c\alpha_t|1\rangle_c|0\rangle_t + \beta_c\beta_t|1\rangle_c|1\rangle_t) \\ & - \frac{(1+r)r^2\beta_p}{2\sqrt{2}}|\psi\rangle|V\rangle(\alpha_c\alpha_t|0\rangle_c|1\rangle_t + \alpha_c\beta_t|0\rangle_c|0\rangle_t) \\ & + \frac{(1-r)r^2\beta_p}{2\sqrt{2}}|\psi\rangle|V\rangle(\beta_c\alpha_t|1\rangle_c|1\rangle_t + \beta_c\beta_t|1\rangle_c|0\rangle_t).\end{aligned} \quad (21)$$

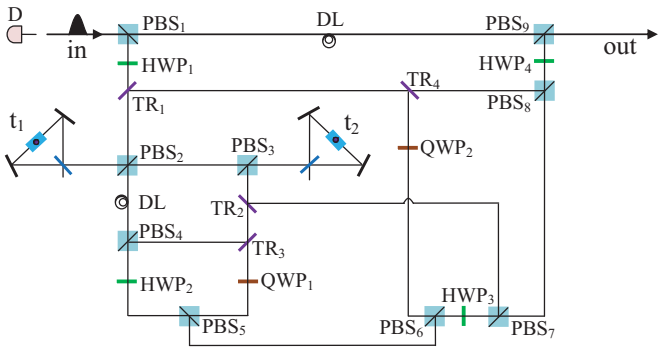

FIG. 4. Schematic setup for realizing a three-qubit Fredkin gate with a flying photon as the control qubit and two emitters confined in 1D waveguides as the target qubits.

Finally, the photon passes through HWP_4 and QWP_4, and interferes with the photon part emitting from PBS_1 in PBS_8. That is, the state of the hybrid system evolves into

$$\begin{aligned}|\Phi_5\rangle =& \alpha_p|\psi\rangle|H\rangle(\alpha_c|0\rangle+\beta_c|1\rangle)_c(\alpha_t|0\rangle+\beta_t|1\rangle)_t\\ &+\frac{\beta_p|\psi\rangle}{4}\{[(1-r)^2|V\rangle+(1-r^2)|H\rangle]\\ &\otimes(\alpha_c\alpha_t|0\rangle_c|0\rangle_t+\alpha_c\beta_t|0\rangle_c|1\rangle_t)\\ &+[(1+r)^2|V\rangle+(1-r^2)|H\rangle]\\ &\otimes(\beta_c\alpha_t|1\rangle_c|0\rangle_t+\beta_c\beta_t|1\rangle_c|1\rangle_t)\\ &-[r(1+r)^2|V\rangle+r(1-r^2)|H\rangle]\\ &\otimes(\alpha_c\alpha_t|0\rangle_c|1\rangle_t+\alpha_c\beta_t|0\rangle_c|0\rangle_t)\\ &-[r(1-r)^2|V\rangle+r(1-r^2)|H\rangle]\\ &\otimes(\beta_c\alpha_t|1\rangle_c|1\rangle_t+\beta_c\beta_t|1\rangle_c|0\rangle_t)\}. \end{aligned} \tag{22}$$

For a perfect scattering process, i.e., $r=-1$, the above state becomes

$$\begin{aligned}|\Phi_6\rangle =& \alpha_p\alpha_c|\psi\rangle|H\rangle|0\rangle_c(\alpha_t|0\rangle+\beta_t|1\rangle)_t\\ &+\alpha_p\beta_c|\psi\rangle|H\rangle|1\rangle_c(\alpha_t|0\rangle+\beta_t|1\rangle)_t\\ &+\beta_p\alpha_c|\psi\rangle|V\rangle|0\rangle_c(\alpha_t|0\rangle+\beta_t|1\rangle)_t\\ &+\beta_p\beta_c|\psi\rangle|V\rangle|1\rangle_c(\alpha_t|1\rangle+\beta_t|0\rangle)_t. \end{aligned} \tag{23}$$

From Eq. (23), one can see that the state of the target qubit is flipped only when the photon is in the state $|V\rangle$ and the control qubit is in the state $|1\rangle$. That is, the schematic setup shown in Fig. 3 can realize a Toffoli gate on a photon-emitter-emitter hybrid system. Moreover, our Toffoli gate works in a heralded way, assisted by the photon detectors D_1, D_2, and D_3. That is, when the faulty scattering event between the photon and emitter c (emitter t) occurs, the photon detector clicks.

V. FREDKIN GATE ON A THREE-QUBIT HYBRID SYSTEM

A Fredkin gate for a hybrid system is used to complete a swap operation on two target qubits when the control photonic qubit is in the state $|V\rangle$. The schematic setup for our Fredkin gate is shown in Fig. 4. In the following, we will describe how to construct this three-qubit gate.

Suppose that the initial states of the flying photon qubit and two target qubits t_1 and t_2 are prepared in $|\varphi\rangle_p=\alpha_p|H\rangle+\beta_p|V\rangle$, $|\varphi\rangle_{t_1}=\alpha_1|0\rangle_{t_1}+\beta_1|1\rangle_{t_1}$ and $|\varphi\rangle_{t_2}=\alpha_2|0\rangle_{t_2}+\beta_2|1\rangle_{t_2}$, respectively. Here, $|\alpha_p|^2+|\beta_p|^2=|\alpha_1|^2+|\beta_1|^2=|\alpha_2|^2+|\beta_2|^2=1$. That is, the initial state of the whole hybrid system can be written as

$$|\Omega_0\rangle=|\psi\rangle|\varphi\rangle_p\otimes|\varphi\rangle_{t_1}\otimes|\varphi\rangle_{t_2}, \tag{24}$$

where $|\psi\rangle$ denotes the spatial wave function of the incident photon.

First, the input photon is split into two wave packets by PBS_1. The part in the state $|H\rangle$ passes through PBS_1, and arrives in PBS_9 directly. The part in the state $|V\rangle$ is reflected by PBS_1, and goes through HWP_1 and TR_1 (transmit). After the above operations, the state of the system evolves into

$$\begin{aligned}|\Omega_1\rangle =& \alpha_p|\psi\rangle|H\rangle(\alpha_1|0\rangle+\beta_1|1\rangle)_{t_1}(\alpha_2|0\rangle+\beta_2|1\rangle)_{t_2}\\ &+\frac{\beta_p}{\sqrt{2}}|\psi\rangle(|H\rangle-|V\rangle)(\alpha_1|0\rangle+\beta_1|1\rangle)_{t_1}\\ &\otimes(\alpha_2|0\rangle+\beta_2|1\rangle)_{t_2}. \end{aligned} \tag{25}$$

Second, after passing through TR_1 (transmit), the photon component is split into two parts by PBS_2. The part in the state $|H\rangle$ travels through PBS_2, and arrives in PBS_4 directly. While the part in the state $|V\rangle$ experiences a series of operations as follows: $PBS_2\rightarrow$ emitter $t_1\rightarrow PBS_2\rightarrow PBS_3\rightarrow$ emitter $t_2\rightarrow PBS_3\rightarrow TR_2$(transmit) $\rightarrow TR_3$(reflect) $\rightarrow PBS_4$. After the two parts get together in PBS_4, the state of the whole system becomes

$$\begin{aligned}|\Omega_2\rangle =& \alpha_p|\psi\rangle|H\rangle(\alpha_1|0\rangle+\beta_1|1\rangle)_{t_1}(\alpha_2|0\rangle+\beta_2|1\rangle)_{t_2}\\ &+\frac{\beta_p}{\sqrt{2}}|\psi\rangle|H\rangle(\alpha_1|0\rangle+\beta_1|1\rangle)_{t_1}(\alpha_2|0\rangle+\beta_2|1\rangle)_{t_2}\\ &-\frac{r^2\beta_p}{\sqrt{2}}|\psi\rangle|V\rangle(\alpha_1|0\rangle-\beta_1|1\rangle)_{t_1}(\alpha_2|0\rangle-\beta_2|1\rangle)_{t_2}. \end{aligned} \tag{26}$$

Then, the photon goes through HWP_2, and the state of the hybrid system becomes

$$\begin{aligned}|\Omega_3\rangle =& \alpha_p|\psi\rangle|H\rangle(\alpha_1|0\rangle+\beta_1|1\rangle)_{t_1}(\alpha_2|0\rangle+\beta_2|1\rangle)_{t_2}\\ &+\frac{\beta_p|\psi\rangle}{2}\{|H\rangle[(1-r^2)\alpha_1\alpha_2|00\rangle+(1+r^2)\alpha_1\beta_2|01\rangle\\ &+(1+r^2)\beta_1\alpha_2|10\rangle+(1-r^2)\beta_1\beta_2|11\rangle]_{t_1t_2}\\ &+|V\rangle[(1+r^2)\alpha_1\alpha_2|00\rangle+(1-r^2)\alpha_1\beta_2|01\rangle\\ &+(1-r^2)\beta_1\alpha_2|10\rangle+(1+r^2)\beta_1\beta_2|11\rangle]_{t_1t_2}\}. \end{aligned} \tag{27}$$

Third, the photon emitting from HWP_2 is split into two wave packets by PBS_5. The part in the state $|V\rangle$ is reflected by PBS_5, and arrives in PBS_6 directly. While the part in the state $|H\rangle$ experiences a series of operations as follows: $PBS_5\rightarrow QWP_1\rightarrow TR_3$(transmit) $\rightarrow TR_2$(transmit) $\rightarrow PBS_3\rightarrow$ emitter $t_2\rightarrow PBS_3\rightarrow PBS_2\rightarrow$ emitter $t_1\rightarrow PBS_2\rightarrow TR_1$ (reflect) $\rightarrow TR_4$(reflect) $\rightarrow QWP_2\rightarrow PBS_6$. Note that, before and after the interaction between the photon and the target emitter t_1 (t_2), a Hadamard operation is performed on emitter t_1 (t_2). After the two parts get together at PBS_6, the state of the whole system evolves into

$$\begin{aligned}|\Omega_4\rangle =& \alpha_p|\psi\rangle|H\rangle(\alpha_1|0\rangle+\beta_1|1\rangle)_{t_1}(\alpha_2|0\rangle+\beta_2|1\rangle)_{t_2}\\ &+\frac{\beta_p|\psi\rangle}{2}|V\rangle[(1+r^2)\alpha_1\alpha_2|00\rangle+(1-r^2)\alpha_1\beta_2|01\rangle \end{aligned}$$

$$+(1-r^2)\beta_1\alpha_2|10\rangle+(1+r^2)\beta_1\beta_2|11\rangle]_{t_1t_2}.$$
$$+\frac{r^2\beta_p|\psi\rangle}{2}|H\rangle[(1-r^2)\alpha_1\alpha_2|11\rangle+(1+r^2)\alpha_1\beta_2|10\rangle$$
$$+(1+r^2)\beta_1\alpha_2|01\rangle+(1-r^2)\beta_1\beta_2|00\rangle]_{t_1t_2}. \quad (28)$$

Fourth, the photon emitting from PBS_6 passes through HWP_3, and is split into two wave packets by PBS_7. The part in the state $|H\rangle$ goes through PBS_7, and arrives in PBS_8 directly. While the part in the state $|V\rangle$ is reflected by PBS_7 and experiences a series of operations as follows: TR_2(reflect) $\rightarrow$ PBS_3 $\rightarrow$ emitter t_2 $\rightarrow$ PBS_3 $\rightarrow$ PBS_2 $\rightarrow$ emitter t_1 $\rightarrow$ PBS_2 $\rightarrow$ TR_1 (reflect) $\rightarrow$ TR_4 (transmit) $\rightarrow$ PBS_8. After the two parts get together at PBS_6, the state of the hybrid system becomes

$$\begin{aligned}|\Omega_5\rangle=&\alpha_p|\psi\rangle|H\rangle(\alpha_1|0\rangle+\beta_1|1\rangle)_{t_1}(\alpha_2|0\rangle+\beta_2|1\rangle)_{t_2}\\&+\frac{\beta_p|\psi\rangle}{2\sqrt{2}}|H\rangle\{[(1+r^2)\alpha_1\alpha_2+(1-r^2)\beta_1\beta_2]|00\rangle\\&+[(1-r^2)\alpha_1\beta_2+(1+r^2)\beta_1\alpha_2]|01\rangle\\&+[(1-r^2)\beta_1\alpha_2+(1+r^2)\alpha_1\beta_2]|10\rangle\\&+[(1+r^2)\beta_1\beta_2+(1-r^2)\alpha_1\alpha_2]|11\rangle]\}_{t_1t_2}\\&+\frac{r^2\beta_p|\psi\rangle}{2\sqrt{2}}|V\rangle\{[r^2(1-r^2)\beta_1\beta_2-(1+r^2)\alpha_1\alpha_2]|00\rangle\\&+[(1-r^2)\alpha_1\beta_2-r^2(1+r^2)\beta_1\alpha_2]|01\rangle\\&+[(1-r^2)\beta_1\alpha_2-r^2(1+r^2)\alpha_1\beta_2]|10\rangle\\&+[r^2(1-r^2)\alpha_1\alpha_2-(1+r^2)\beta_1\beta_2]|11\rangle]\}_{t_1t_2}. \quad (29)\end{aligned}$$

Finally, the photon emitting from PBS_8 passes through HWP_4, and gets together at PBS_8 with the photon emitting from PBS_1. After the above processes, the state of the hybrid system evolves into

$$\begin{aligned}|\Omega_6\rangle=&\alpha_p|\psi\rangle|H\rangle(\alpha_1|0\rangle+\beta_1|1\rangle)_{t_1}(\alpha_2|0\rangle+\beta_2|1\rangle)_{t_2}\\&+\frac{\beta_p|\psi\rangle}{4}(|H\rangle+|V\rangle)\\&\otimes\{[(1+r^2)\alpha_1\alpha_2+(1-r^2)\beta_1\beta_2]|00\rangle\\&+[(1-r^2)\alpha_1\beta_2+(1+r^2)\beta_1\alpha_2]|01\rangle\\&+[(1-r^2)\beta_1\alpha_2+(1+r^2)\alpha_1\beta_2]|10\rangle\\&+[(1+r^2)\beta_1\beta_2+(1-r^2)\alpha_1\alpha_2]|11\rangle]\}_{t_1t_2}\\&+\frac{r^2\beta_p|\psi\rangle}{4}(|H\rangle-|V\rangle)\\&\otimes\{[r^2(1-r^2)\beta_1\beta_2-(1+r^2)\alpha_1\alpha_2]|00\rangle\\&+[(1-r^2)\alpha_1\beta_2-r^2(1+r^2)\beta_1\alpha_2]|01\rangle\\&+[(1-r^2)\beta_1\alpha_2-r^2(1+r^2)\alpha_1\beta_2]|10\rangle\\&+[r^2(1-r^2)\alpha_1\alpha_2-(1+r^2)\beta_1\beta_2]|11\rangle]\}_{t_1t_2}. \quad (30)\end{aligned}$$

For a perfect scattering process, i.e., $r=-1$, the above state evolves into

$$\begin{aligned}|\Omega_7\rangle=&\alpha_p|\psi\rangle|H\rangle(\alpha_1|0\rangle+\beta_1|1\rangle)_{t_1}(\alpha_2|0\rangle+\beta_2|1\rangle)_{t_2}\\&+\beta_p|\psi\rangle|V\rangle(\alpha_2|0\rangle+\beta_2|1\rangle)_{t_1}(\alpha_1|0\rangle+\beta_1|1\rangle)_{t_2}. \quad (31)\end{aligned}$$

From Eq. (31), one can see that the states of the two target qubits are swapped when the photon qubit is in the state $|V\rangle$, while nothing is done when photon qubit is in the state $|H\rangle$. That is, the quantum circuit shown in Fig. 4 can realize a Fredkin gate on a photon-emitter-emitter hybrid system.

VI. DISCUSSION AND CONCLUSION

We have proposed some heralded schemes for implementing quantum gates, including CNOT, Toffoli, and Fredkin gates. The control qubit of the gates in our scheme is encoded on the flying photon, and the target qubits are encoded on the emitters coupled to 1D waveguides. The performance of our gates depends on the scattering configuration shown in Fig. 1(b). Its success probability can be defined as $p_0=|\langle\psi|\phi_r\rangle|^2$, where $|\psi\rangle$ and $|\phi_r\rangle$ are the spatial wave functions of the input photon and the photon component reflected by the emitter in the 1D waveguide, respectively. In a realistic emitter-waveguide system, the Purcell factor is finite and $|\phi_r\rangle\neq-|\psi\rangle$. In particular, the faulty scattering event is tagged with an unchanged polarization state, which can be discarded assisted by PBS and single-photon detector.

Since the scattering setup shown in Fig. 1(b) is the core of our schemes for the three quantum gates, we discuss its feasibility with current experimental technology. As shown in Fig. 5(a), the platform for emitter-photon scattering can be realized by coupling single quantum dots to photonic crystal waveguides, where $P>20$ can be obtained [96]. In their experiment, the observed decay rate of quantum dots into the waveguide modes is $\gamma_{1D}=1.1$GHz, so that the input photon with pulse duration being around tens of nanoseconds can scatter with the emitter in an excellent reflection fidelity. The Hadamard operations on the states of the emitters can be accomplished in picoseconds [89]. Also, in the core scattering setups of Figs. 2–4, i.e., the triangular structure BS-M_1-M_2 in Fig. 1(b), the length of the loop needs to be significantly larger than the size of the input photon wave packet, so that beam splitter can effectively split up the wave packet into a temporal order as we wanted in our protocols. Not surprisingly the free space photon paths shown in our schemes can be integrated onto a single chip [97]. Thus, considering all optical elements, the total duration of our gates would be comparable to the coherence time $T\sim2.6\mu$s of bare quantum dots [98]. Even though, the coherence time of quantum dots can be enhanced dramatically by controlling the surrounding nuclear-spin bath [99].

In our protocols for CNOT, Toffoli, and Fredkin gates, physical errors caused by system imperfections, such as frequency detunings, weak couplings, and finite bandwidths of the input photonic pulses, can be mapped into the detection of photon polarization. In our system, the decoherence of the emitter is mainly the emission or scattering to undesired modes. This induces the faulty scattering event, which can also be tagged and discarded by detecting the polarization states of output photons. While, photon loss in the scattering setup can not be heralded. Even though, we can adopt specific single-photon sources, which generate photons pairs via parametric down-conversion in bulk crystals [100] or waveguides [101]. In such cases, since the photons are created in pairs, one photon can be used to encode quantum qubit and

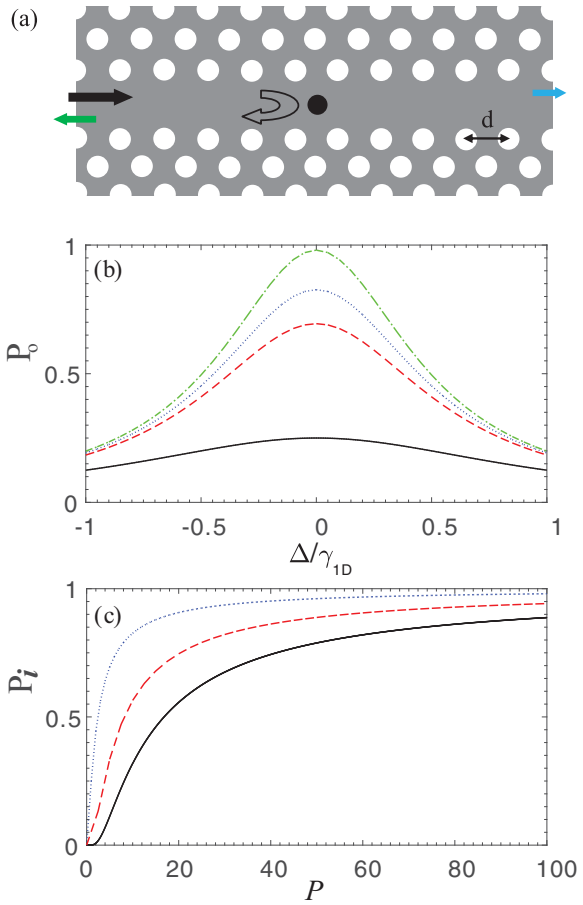

FIG. 5. (a) Schematic of an input photon scatters with a quantum dot (black dot) coupled to a 1D slow-light photonic crystal waveguide with lattice constant d. The arrows denote the input field (black), reflected field (green) and transmitted field (blue). (b) The success probabilities of the scattering configuration shown in Fig. 1(b) versus frequency detuning Δ/γ_{1D} for the Purcell factor $P = 1.0$ (black solid line), $P = 5.0$ (red dashed line), $P = 10$ (blue dotted line), $P = 100$ (green dashed-dotted line). (c) The success probabilities versus the Purcell factor P for CNOT (black solid line), Toffoli (red dashed line), and Fredkin (blue dotted line) gates with $\Delta = 0$.

another one can be used to herald the loss of the photonic qubit. This can effectively weaken the influence of photon loss on the construction of quantum gates in our scheme. In addition, there are two arms in our protocols: one arm contains scattering events and another not. Thus, the need to balance photon losses in the two arms is very important for our schemes to achieve high fidelities. For successful events of imperfect scattering processes, i.e., the polarization state is swapped but $|\phi_r\rangle \neq -|\psi\rangle$ in Eqs. (9) and (10), the spatial wave functions of the wave packets meeting at the final PBS (e.g., PBS_3 in Fig. 2) in our protocols no longer coincide. To compensate for this, we can add a wave-form corrector in the arm containing no scattering events in our schemes, e.g., in the path between PBS_1 and PBS_3 in Fig. 2. In the experiment, when the bandwidth of the incident photon is much narrower than γ_{1D}, it can be regarded as a plane wave. Thus, the wave form in the arm with scattering events can be mapped to $k|\psi\rangle$, where $|k| < 1$. In detail, when the incident photon is resonant with the emitters, $0 \leqslant |k| < 1$, and the wave-form corrector in the arm with no scattering events only includes an attenuator, whose transmissivity is k. Meanwhile, when the frequency detuning between the incident photon and the emitters is not zero, k is a complex number, and the wave-form corrector contains a phase modulator.

As shown in Fig. 5(b), we give the success probabilities of the scattering configuration in Fig. 1(b) as a function of the frequency detuning Δ/γ_{1D} for four choices of the Purcell factor. In fact, according to the descriptions given in Sec. II, the success probability of the basic scattering configuration is $p_0 = |r|^2$. The results show that, for a fixed Purcell factor, the success probability p_0 decreases with the increment of the frequency detuning Δ/γ_{1D}. In addition, we also find that the success probability is improved remarkably when we increase the Purcell factor. For example, we can obtain $p_0 = 92.56\%$ with the parameters $P = 50$ and $\Delta/\gamma_{1D} = 0.1$. Moreover, we compute the success probabilities of our schemes for CNOT, Toffoli, and Fredkin gates with $\Delta = 0$, as shown in Fig. 5(c). Owing to the heralded mechanism, only when all the scattering events between flying photons and emitters in 1D waveguides happen in our schemes, can we obtain the three quantum gates successfully. In fact, our protocols for realizing CNOT, Toffoli, and Fredkin gates contain one, three, and six basic scattering events, respectively. Therefore, the success probabilities of our CNOT, Toffoli, and Fredkin gates are p_0, p_0^3, and p_0^6, respectively. The results show that the success probabilities of the three quantum gates rise obviously when we enhance the Purcell factor. Recently, great progress has been made to realize strong coupling between emitters and 1D waveguides. For example, by placing a single quantum dot at an optimal position in the system, Kolchin *et al.* [102] demonstrated strong optical interactions and emission coupling, where a high Purcell factor $P = 31$ can be experimentally realized. With $P = 31$, the success probabilities of our CNOT, Toffoli, and Fredkin gates are $p_1 = 93.9\%$, $p_2 = 82.7\%$ and $p_3 = 68.3\%$, respectively.

Taking no account of the heralded mechanism, we discuss the fidelities of our quantum gates. The fidelity of a quantum gate can be defined as $F = |\langle\Psi_r|\Psi_i\rangle|^2$, where $|\Psi_r\rangle$ and $|\Psi_i\rangle$ denote the final states of the hybrid systems in the realistic case and the ideal case, respectively. In detail, the fidelities of our CNOT, Toffoli, and Fredkin gates are $F_C = |\langle\Psi_4|\Psi_5\rangle|^2$, $F_T = |\langle\Phi_5|\Phi_6\rangle|^2$, and $F_F = |\langle\Omega_6|\Omega_7\rangle|^2$, respectively. As shown in Fig. 6, we give the fidelities of our three quantum gates as a function of the frequency detuning Δ/γ_{1D} and the Purcell factor P. The results of Fig. 6(a) show that, for a fixed Purcell factor, the fidelities of our three quantum gates decrease with the increment of the frequency detuning. For example, for $\Delta = 0$ with the Purcell factor $P = 100$, the fidelities of our three gates are $F_C = 99.02\%$, $F_T = 98.62\%$ and $F_F = 98.96\%$, respectively. While, for $\Delta = 0.1\gamma_{1D}$ with $P = 100$, the fidelities of our three gates turn to be $F_C = 96.55\%$, $F_T = 91.96\%$ and $F_F = 92.65\%$, respectively. The results of Fig. 6(b) reveal that, for a fixed frequency detuning, the fidelities of the three gates are greatly improved by the increment of the Purcell factor. For example, for the case $P = 30$ with $\Delta = 0$, the fidelities of our three gates are $F_C = 96.70\%$, $F_T = 95.73\%$, and $F_F = 97.07\%$, respectively.

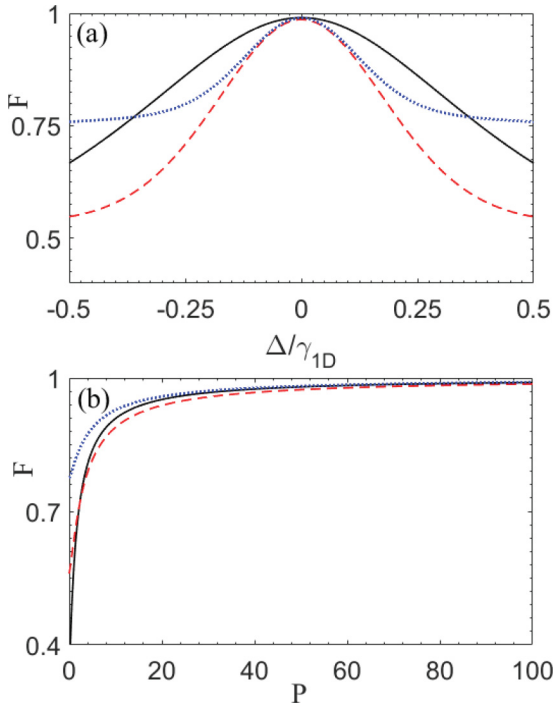

FIG. 6. The fidelities of the CNOT gate (black solid line), Toffoli gate (red dashed line), and Fredkin gate (blue dotted line) as a function of (a) the frequency detuning Δ/γ_{1D} and (b) the Purcell factor P. Parameters: (a) $P = 100$, (b) $\Delta = 0$.

While, for $P = 80$ with $\Delta = 0$, the fidelities of our three gates become $F_C = 98.73\%$, $F_T = 98.32\%$, and $F_F = 98.82\%$, respectively. Thus, to obtain high fidelities, the frequency detuning between the incident photons and the emitters should be sufficiently small and the Purcell factor is sufficiently large.

In practical systems, inhomogeneous broadening exists in the transitions of the emitters [103,104]. For concreteness, we assume that the inhomogeneous broadening is Gaussian with the probability density $\rho_{ih}(\Delta_{ih}) = \frac{1}{\sqrt{2\pi}\sigma_{ih}} \exp(-\frac{\Delta_{ih}^2}{2\sigma_{ih}^2})$, where Δ_{ih} is the inhomogeneous detuning from the expected frequency of the transition and $2\sigma_{ih}$ is the full width at half maximum of the line shape in inhomogeneous broadening. As shown in Fig. 7, we give the fidelities of our three gates in four cases, i.e., $\sigma_{ih} = 0$, $0.1\gamma_{1D}$, $0.2\gamma_{1D}$, $0.3\gamma_{1D}$. The results reveal that, for the three quantum gates, the existence of inhomogeneous broadening decreases the fidelities, which indicates that the inhomogeneous broadening destroys the perfect scattering processes between the photon wave packets and emitters. Moreover, with the increment of the parameter σ_{ih}, the fidelities of the three gates decrease obviously for a fixed detuning. Also, for the three gates, the influence of the inhomogeneous broadening on the fidelities decreases when the frequency detuning between the photon and emitters rises. As shown in Fig. 6(a), high fidelities are obtained when the detuning is sufficiently small. Therefore, to obtain high fidelities, the inhomogeneous broadening needs to be strongly suppressed.

In conclusion, we have proposed some heralded protocols for constructing CNOT, Toffoli, and Fredkin gates on photon-emitter hybrid systems, by utilizing the photon scattering off

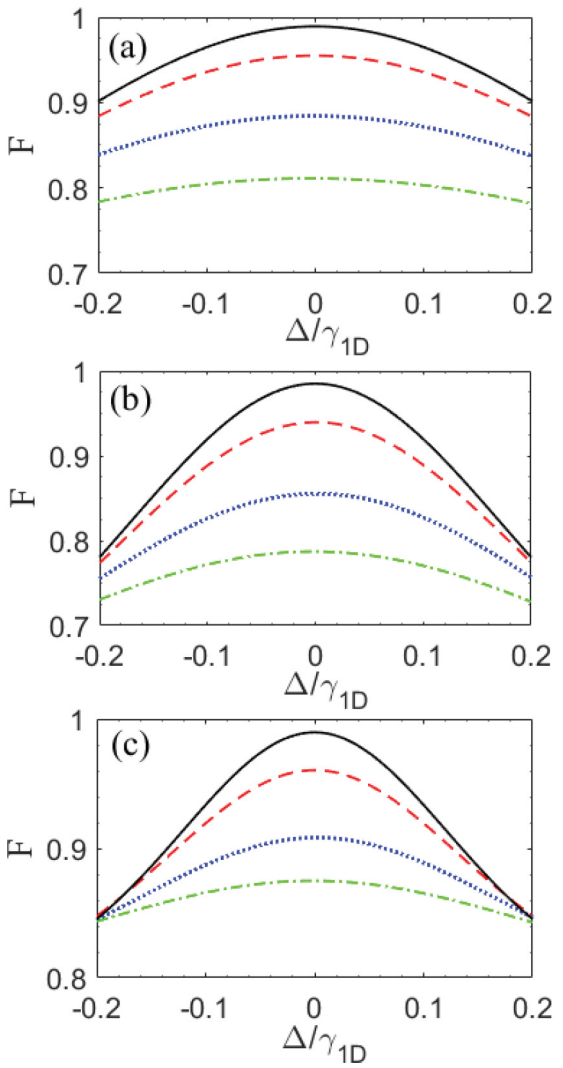

FIG. 7. The fidelities of (a) the CNOT gate, (b) Toffoli gate, and (c) Fredkin gate as a function of Δ/γ_{1D} for $\sigma_{ih} = 0$ (black solid lines), $\sigma_{ih} = 0.1\gamma_{1D}$ (red dashed lines), $\sigma_{ih} = 0.2\gamma_{1D}$ (blue dotted lines), $\sigma_{ih} = 0.3\gamma_{1D}$ (green dashed-dotted lines). (a)–(c) $P = 100$.

single emitters coupled to 1D waveguides. In our schemes, faulty scattering events between flying photons and emitters in 1D waveguides can be tagged and discarded, which provides an advantageous approach for constructing quantum gates. Therefore, our schemes for the three quantum gates are implemented in a heralded manner, which is advantageous for quantum information. With great progress in emitter-waveguide systems, the devices for the three quantum gates is feasible in experiment.

ACKNOWLEDGMENTS

We thank M. J. Tao and J. Qiu for stimulating discussions. This work is supported by the National Natural Science Foundation of China (NSFC) under Grants No. 12004281, No. 11947037, No. 11704214, and No. 11604012, the Program for Innovative Research in University of Tianjin under Grant No. TD13-5077 and the Fundamental Research Funds for the Central Universities under Grant No.

FRF-BR-17-004B. G.-L.L. acknowledges support from the Center of Atomic and Molecular Nanosciences, Tsinghua University, and Beijing Advanced Innovation Center for Future Chip (ICFC).

[1] M. A. Nielsen and I. L. Chuang, *Quantum Computation and Quantum Information* (Cambridge University Press, Cambridge, 2000).

[2] D. P. DiVincenzo, Two-bit gates are universal for quantum computation, Phys. Rev. A **51**, 1015 (1995).

[3] A. Barenco, C. H. Bennett, R. Cleve, D. P. DiVincenzo, N. Margolus, P. Shor, T. Sleator, J. A. Smolin, and H. Weinfurter, Elementary gates for quantum computation, Phys. Rev. A **52**, 3457 (1995).

[4] E. Knill, R. Laflamme, and G. J. Milburn, A scheme for efficient quantum computation with linear optics, Nature (London) **409**, 46 (2001).

[5] L. M. Duan and H. J. Kimble, Scalable Photonic Quantum Computation Through Cavity-Assisted Interactions, Phys. Rev. Lett. **92**, 127902 (2004).

[6] G. L. Long, General quantum interference principle and duality computer, Commun. Theor. Phys. **45**, 825 (2006).

[7] A. Reiserer, N. Kalb, G. Rempe, and S. Ritter, A quantum gate between a flying optical photon and a single trapped atom, Nature (London) **508**, 237 (2014).

[8] T. G. Tiecke, J. D. Thompson, N. P. de Leon, L. R. Liu, V. Vuletic, and M. D. Lukin, Nanophotonic quantum phase switch with a single atom, Nature (London) **508**, 241 (2014).

[9] M. Veldhorst, C. Yang, J. Hwang *et al.*, A two-qubit logic gate in silicon, Nature (London) **526**, 410 (2015).

[10] B. Hacker, S. Welte, G. Rempe, and S. Ritter, A photon-photon quantum gate based on a single atom in an optical resonator, Nature (London) **536**, 193 (2016).

[11] X. Qiang, X. Zhou, J. Wang, C. M. Wilkes, T. Loke, S. O'Gara, L. Kling, G. D. Marshall, R. Santagati, T. C. Ralph *et al.*, Large-scale silicon quantum photonics implementing arbitrary two-qubit processing, Nat. Photon. **12**, 534 (2018).

[12] D. Tiarks, S. Schmidt-Eberle, T. Stolz, G. Rempe, and S. Dürr, A photon-photon quantum gate based on Rydberg interactions, Nat. Phys. **15**, 124 (2019).

[13] H. Levine, A. Keesling, G. Semeghini, A. Omran, T. T. Wang, S. Ebadi, H. Bernien, M. Greiner, V. Vuletić, H. Pichler, and M. D. Lukin, Parallel Implementation of High-Fidelity Multiqubit Gates with Neutral Atoms, Phys. Rev. Lett. **123**, 170503 (2019).

[14] E. Fredkin and T. Toffoli, Conservative logic, Int. J. Theor. Phys. **21**, 219 (1982).

[15] P. W. Shor, Polynomial-time algorithms for prime factorization and discrete logarithms on a quantum computer, SIAM J. Comput. **26**, 1484 (1997).

[16] L. K. Grover, Quantum Mechanics Helps in Searching for a Needle in a Haystack, Phys. Rev. Lett. **79**, 325 (1997).

[17] G. L. Long, Grover algorithm with zero theoretical failure rate, Phys. Rev. A **64**, 022307 (2001).

[18] R. Cleve, A. Ekert, C. Macchiavello, and M. Mosca, Quantum algorithms revisited, Proc. R. Soc. A **454**, 339 (1998).

[19] D. Loss and D. P. DiVincenzo, Quantum computation with quantum dots, Phys. Rev. A **57**, 120 (1998).

[20] X. Li, Y. Wu, D. Steel, D. Gammon, T. H. Stievater, D. S. Katzer, D. Park, C. Piermarocchi, and L. J. Sham, An all-optical quantum gate in a semiconductor quantum dot, Science **301**, 809 (2003).

[21] C. Y. Hu, A. Young, J. L. O'Brien, W. J. Munro, and J. G. Rarity, Giant optical Faraday rotation induced by a single-electron spin in a quantum dot: Applications to entangling remote spins via a single photon, Phys. Rev. B **78**, 085307 (2008).

[22] H. F. Wang, A. D. Zhu, S. Zhang, and K. H. Yeon, Optically controlled phase gate and teleportation of a controlled-not gate for spin qubits in a quantum-dot-microcavity coupled system, Phys. Rev. A **87**, 062337 (2013).

[23] H. R. Wei and F. G. Deng, Universal quantum gates for hybrid systems assisted by quantum dots inside double-sided optical microcavities, Phys. Rev. A **87**, 022305 (2013).

[24] W. Q. Liu and H. R. Wei, Implementations of more general solid-state $(\mathrm{SWAP})^{1/m}$ and controlled-$(\mathrm{swap})^{1/m}$ gates, New J. Phys. **21**, 103018 (2019).

[25] T. Yamamoto, Y. A. Pashkin, O. Astafiev, Y. Nakamura, and J. S. Tsai, Demonstration of conditional gate operation using superconducting charge qubits, Nature (London) **425**, 941 (2003).

[26] L. DiCarlo, J. M. Chow, J. M. Gambetta, L. S. Bishop, B. R. Johnson, D. I. Schuster, J. Majer, A. Blais, L. Frunzio, S. M. Girvin, and R. J. Schoelkopf, Demonstration of two-qubit algorithms with a superconducting quantum processor, Nature (London) **460**, 240 (2009).

[27] M. Neeley, R. C. Bialczak, M. Lenander, E. Lucero, M. Mariantoni, A. O'connell, D. Sank, H. Wang, M. Weides, J. Wenner *et al.*, Generation of three-qubit entangled states using superconducting phase qubits, Nature (London) **467**, 570 (2010).

[28] G. Romero, D. Ballester, Y. M. Wang, V. Scarani, and E. Solano, Ultrafast Quantum Gates in Circuit QED, Phys. Rev. Lett. **108**, 120501 (2012).

[29] R. Barends, J. Kelly, A. Megrant, A. Veitia, D. Sank, E. Jeffrey, T. C. White, J. Mutus, A. G. Fowler, B. Campbell *et al.*, Superconducting quantum circuits at the surface code threshold for fault tolerance, Nature (London) **508**, 500 (2014).

[30] C. K. Andersen and K. Mølmer, Multifrequency modes in superconducting resonators: Bridging frequency gaps in off-resonant couplings, Phys. Rev. A **91**, 023828 (2015).

[31] G. L. Long and L. Xiao, Experimental realization of a fetching algorithm in a 7-qubit NMR spin Liouville space computer, J. Chem. Phys. **119**, 8473 (2003).

[32] J. A. Jones, M. Mosca, and R. H. Hansen, Implementation of a quantum search algorithm on a quantum computer, Nature (London) **393**, 344 (1998).

[33] G. R. Feng, G. F. Xu, and G. L. Long, Experimental Realization of Nonadiabatic Holonomic Quantum Computation, Phys. Rev. Lett. **110**, 190501 (2013).

[34] T. Xin, L. Hao, S. Y. Hou, G. R. Feng, and G. L. Long, Preparation of pseudo-pure states for NMR quantum computing with one ancillary qubit, Sci. China-Phys. Mech. Astron. **62**, 960312 (2019).

[35] E. Togan, Y. Chu, A. S. Trifonov, L. Jiang, J. Maze, L. Childress, M. V. G. Dutt, A. S. Sørensen, P. R. Hemmer, A. S. Zibrov, and M. D. Lukin, Quantum entanglement between an

optical photon and a solid-state spin qubit, Nature (London) **466**, 730 (2010).

[36] H. R. Wei and F. G. Deng, Compact quantum gates on electron-spin qubits assisted by diamond nitrogen-vacancy centers inside cavities, Phys. Rev. A **88**, 042323 (2013).

[37] T. J. Wang and C. Wang, Universal hybrid three-qubit quantum gates assisted by a nitrogen-vacancy center coupled with a whispering-gallery-mode microresonator, Phys. Rev. A **90**, 052310 (2014)

[38] H. R. Wei and G. L. Long, Hybrid quantum gates between flying photon and diamond nitrogen-vacancy centers assisted by optical microcavities, Sci. Rep. **5**, 12918 (2015).

[39] C. Bonato, F. Haupt, S. S. R. Oemrawsingh, J. Gudat, D. Ding, M. P. vanExter, and D. Bouwmeester, CNOT and Bell-State Analysis in the Weak-Coupling Cavity QED Regime, Phys. Rev. Lett. **104**, 160503 (2010).

[40] A. Fedorov, L. Steffen, M. Baur, M. P. da Silva, and A. Wallraff, Implementation of a Toffoli gate with superconducting circuits, Nature (London) **481**, 170 (2011).

[41] R. B. Patel, J. Ho, F. Ferreyrol, T. C. Ralph, and G. J. Pryde, A quantum Fredkin gate, Sci. Adv. **2**, e1501531 (2016).

[42] W. Q. Liu and H. R. Wei, Optimal synthesis of the Fredkin gate in a multilevel system, New J. Phys. **22**, 063026 (2020).

[43] M. Bajcsy, S. Hofferberth, V. Balic, T. Peyronel, M. Hafezi, A. S. Zibrov, V. Vuletic, and M. D. Lukin, Efficient All-Optical Switching Using Slow Light within a Hollow Fiber, Phys. Rev. Lett. **102**, 203902 (2009).

[44] E. Vetsch, D. Reitz, G. Sagué, R. Schmidt, S. T. Dawkins, and A. Rauschenbeutel, Optical Interface Created by Laser-Cooled Atoms Trapped in the Evanescent Field Surrounding an Optical Nanofiber, Phys. Rev. Lett. **104**, 203603 (2010).

[45] S. Okaba, T. Takano, F. Benabid, T. Bradley, L. Vincetti, Z. Maizelis, V. Yampol'skii, F. Nori, and H. Katori, Lamb-Dicke spectroscopy of atoms in a hollow-core photonic crystal fibre, Nat. Commun. **5**, 4096 (2014).

[46] B. Gouraud, D. Maxein, A. Nicolas, O. Morin, and J. Laurat, Demonstration of a Memory for Tightly Guided Light in an Optical Nanofiber, Phys. Rev. Lett. **114**, 180503 (2015).

[47] H. L. Sørensen, J. B. Béguin, K. W. Kluge, I. Iakoupov, A. S. Sørensen, J. H. Müller, E. S. Polzik, and J. Appel, Coherent Backscattering of Light Off One-Dimensional Atomic Strings, Phys. Rev. Lett. **117**, 133604 (2016).

[48] M. T. Cheng, J. P. Xu, and G. S. Agarwal, Waveguide transport mediated by strong coupling with atoms, Phys. Rev. A **95**, 053807 (2017).

[49] G. Z. Song, E. Munro, W. Nie, F. G. Deng, G. J. Yang, and L. C. Kwek, Photon scattering by an atomic ensemble coupled to a one-dimensional nanophotonic waveguide, Phys. Rev. A **96**, 043872 (2017).

[50] Z. H. Wang, L. Du, Y. Li, and Y. Liu, Phase-controlled single-photon nonreciprocal transmission in a one-dimensional waveguide, Phys. Rev. A **100**, 053809 (2019).

[51] A. V. Akimov, A. Mukherjee, C. L. Yu, D. E. Chang, A. S. Zibrov, P. R. Hemmer, H. Park, and M. D. Lukin, Generation of single optical plasmons in metallic nanowires coupled to quantum dots, Nature (London) **450**, 402 (2007).

[52] D. E. Chang, A. S. Sørensen, E. A. Demler, and M. D. Lukin, A single-photon transistor using nanoscale surface plasmons, Nat. Phys. **3**, 807 (2007).

[53] A. Goban, C. L. Hung, S. P. Yu, J. D. Hood, J. A. Muniz, J. H. Lee, M. J. Martin, A. C. McClung, K. S. Choi, D. E. Chang, O. Painter, and H. J. Kimble, Atom-light interactions in photonic crystals, Nat. Commun. **5**, 3808 (2014).

[54] J. S. Douglas, H. Habibian, C. L. Hung, A. V. Gorshkov, H. J. Kimble, and D. E. Chang, Quantum many-body models with cold atoms coupled to photonic crystals, Nat. Photon. **9**, 326 (2015).

[55] A. González-Tudela, C. L. Hung, D. E. Chang, J. I. Cirac, and H. J. Kimble, Subwavelength vacuum lattices and atom-atom interactions in two-dimensional photonic crystals, Nat. Photon. **9**, 320 (2015).

[56] G. Z. Song, E. Munro, W. Nie, L. C. Kwek, F. G. Deng, and G. L. Long, Photon transport mediated by an atomic chain trapped along a photonic crystal waveguide, Phys. Rev. A **98**, 023814 (2018).

[57] T. M. Babinec, J. M. Hausmann, M. Khan, Y. Zhang, J. R. Maze, P. R. Hemmer, and M. Lončar, A diamond nanowire single-photon source, Nat. Nanotechnol. **5**, 195 (2010).

[58] H. Clevenson, M. E. Trusheim, C. Teale, T. Schröder, D. Braje, and D. Englund, Broadband magnetometry and temperature sensing with a light-trapping diamond waveguide, Nat. Phys. **11**, 393 (2015).

[59] A. Sipahigil, R. E. Evans, D. D. Sukachev, M. J. Burek, J. Borregaard, M. K. Bhaskar, C. T. Nguyen, J. L. Pacheco, H. A. Atikian, C. Meuwly *et al.*, An integrated diamond nanophotonics platform for quantum-optical networks, Science **354**, 847 (2016).

[60] A. Wallraff, D. I. Schuster, A. Blais, L. Frunzio, R. S. Huang, J. Majer, S. Kumar, S. M. Girvin, and R. J. Schoelkopf, Strong coupling of a single photon to a superconducting qubit using circuit quantum electrodynamics, Nature (London) **431**, 162 (2004).

[61] K. Lalumière, B. C. Sanders, A. F. van Loo, A. Fedorov, A. Wallraff, and A. Blais, Input-output theory for waveguide QED with an ensemble of inhomogeneous atoms, Phys. Rev. A **88**, 043806 (2013).

[62] X. Gu, A. F. Kockum, A. Miranowicz, Y. X. Liu, and F. Nori, Microwave photonics with superconducting quantum circuits, Phys. Rep. **718-719**, 1 (2017).

[63] N. M. Sundaresan, R. Lundgren, G. Zhu, A. V. Gorshkov, and A. A. Houck, Interacting Qubit-Photon Bound States with Superconducting Circuits, Phys. Rev. X **9**, 011021 (2019).

[64] G. Z. Song, L. C. Kwek, F. G. Deng, and G. L. Long, Microwave transmission through an artificial atomic chain coupled to a superconducting photonic crystal, Phys. Rev. A **99**, 043830 (2019).

[65] J. T. Shen and S. Fan, Coherent photon transport from spontaneous emission in one-dimensional waveguides, Opt. Lett. **30**, 2001 (2005).

[66] J. T. Shen and S. Fan, Coherent Single Photon Transport in a One-Dimensional Waveguide Coupled with Superconducting Quantum Bits, Phys. Rev. Lett. **95**, 213001 (2005).

[67] Y. Li, L. Aolita, D. E. Chang, and L. C. Kwek, Robust-Fidelity Atom-Photon Entangling Gates in the Weak-Coupling Regime, Phys. Rev. Lett. **109**, 160504 (2012).

[68] K. Kojima, H. F. Hofmann, S. Takeuchi, and K. Sasaki, Nonlinear interaction of two photons with a one-dimensional atom: Spatiotemporal quantum coherence in the emitted field, Phys. Rev. A **68**, 013803 (2003).

[69] E. Waks and J. Vuckovic, Dipole Induced Transparency in Drop-Filter Cavity-Waveguide Systems, Phys. Rev. Lett. **96**, 153601 (2006).

[70] L. Zhou, Z. R. Gong, Y. X. Liu, C. P. Sun, and F. Nori, Controllable Scattering of a Single Photon inside a One-Dimensional Resonator Waveguide, Phys. Rev. Lett. **101**, 100501 (2008).

[71] K. Koshino, S. Ishizaka, and Y. Nakamura, Deterministic photon-photon $\sqrt{SWAP}$ gate using a Λ system, Phys. Rev. A **82**, 010301(R) (2010).

[72] H. Zheng, D. J. Gauthier, and H. U. Baranger, Waveguide-QED-Based Photonic Quantum Computation, Phys. Rev. Lett. **111**, 090502 (2013).

[73] W. B. Yan and H. Fan, Single-photon quantum router with multiple output ports, Sci. Rep. **4**, 4820 (2014).

[74] P. Lodahl, S. Mahmoodian, S. Stobbe, A. Rauschenbeutel, P. Schneeweiss, J. Volz, H. Pichler, and P. Zoller, Chiral quantum optics, Nature (London) **541**, 473 (2017).

[75] T. Li, A. Miranowicz, X. Hu, K. Xia, and F. Nori, Quantum memory and gates using a Λ-type quantum emitter coupled to a chiral waveguide, Phys. Rev. A **97**, 062318 (2018).

[76] K. Xia, F. Nori, and M. Xiao, Cavity-Free Optical Isolators and Circulators Using a Chiral Cross-Kerr Nonlinearity, Phys. Rev. Lett. **121**, 203602 (2018).

[77] D. C. Yang, M. T. Cheng, X. S. Ma, J. Xu, C. J. Zhu, and X. S. Huang, Phase-modulated single-photon router, Phys. Rev. A **98**, 063809 (2018).

[78] C. H. Yan, Y. Li, H. D. Yuan, and L. F. Wei, Targeted photonic routers with chiral photon-atom interactions, Phys. Rev. A **97**, 023821 (2018).

[79] M. Wang, R. Wu, J. Lin, J. Zhang, Z. Fang, Z. Chai, and Y. Cheng, Chemo-mechanical polish lithography: A pathway to low loss large-scale photonic integration on lithium niobate on insulator, Quantum Eng. **1**, e9 (2019).

[80] D. E. Liu, Sensing Kondo correlations in a suspended carbon nanotube mechanical resonator with spin-orbit coupling, Quantum Eng. **1**, e10 (2019).

[81] Z. H. Wang, T. Jaako, P. Kirton, and P. Rabl, Supercorrelated Radiance in Nonlinear Photonic Waveguides, Phys. Rev. Lett. **124**, 213601 (2020).

[82] G. Z. Song, J. L. Guo, W. Nie, L. C. Kwek, and G. L. Long, Optical properties of a waveguide-mediated chain of randomly positioned atoms, Opt. Express **29**, 1903 (2021).

[83] P. Lodahl, S. Mahmoodian, and S. Stobbe, Interfacing single photons and single quantum dots with photonic nanostructures, Rev. Mod. Phys. **87**, 347 (2015).

[84] D. Roy, C. M. Wilson, and O. Firstenberg, Strongly interacting photons in one-dimensional continuum, Rev. Mod. Phys. **89**, 021001 (2017).

[85] D. E. Chang, J. S. Douglas, A. González-Tudela, C.-L. Hung, and H. J. Kimble, Colloquium: Quantum matter built from nanoscopic lattices of atoms and photons, Rev. Mod. Phys. **90**, 031002 (2018).

[86] B. D. Gerardot, D. Brunner, P. A. Dalgarno, P. Öhberg, S. Seidl, M. Kroner, K. Karrai, N. G. Stoltz, P. M. Petroff, and R. J. Warburton, Optical pumping of a single hole spin in a quantum dot, Nature (London) **451**, 441 (2008).

[87] R. J. Warburton, Single spins in self-assembled quantum dots, Nat. Mater. **12**, 483 (2013).

[88] G. Bester, S. Nair, and A. Zunger, Pseudopotential calculation of the excitonic fine structure of million-atom self-assembled $In_{1-x}Ga_xAs$/GaAs quantum dots, Phys. Rev. B **67**, 161306(R) (2003).

[89] J. Berezovsky, M. H. Mikkelsen, N. G. Stoltz, L. A. Coldren, and D. D. Awschalom, Picosecond coherent optical manipulation of a single electron spin in a quantum Dot, Science **320**, 349 (2008).

[90] D. Press, T. D. Ladd, B. Y. Zhang, and Y. Yamamoto, Complete quantum control of a single quantum dot spin using ultrafast optical pulses, Nature (London) **456**, 218 (2008).

[91] C. Santori, D. Fattal, J. Vuckovic, G. S. Solomon, and Y. Yamamoto, Indistinguishable photons from a single-photon device, Nature (London) **419**, 594 (2002).

[92] J. Claudon, J. Bleuse, N. S. Malik, M. Bazin, P. Jaffrennou, N. Gregersen, C. Sauvan, P. Lalanne, and J. M. Gérard, A highly efficient single-photon source based on a quantum dot in a photonic nanowire, Nat. Photonics **4**, 174 (2010).

[93] J. L. O'brien, Optical quantum computing, Science **318**, 1567 (2007).

[94] A. Beveratos, R. Brouri, T. Gacoin, A. Villing, J. P. Poizat, and P. Grangier, Single Photon Quantum Cryptography, Phys. Rev. Lett. **89**, 187901 (2002).

[95] V. Jacques, E. Wu, F. Grosshans, F. Treussart, P. Grangier, A. Aspect, and J. F. Roch, Experimental realization of Wheeler's delayed-choice gedanken experiment, Science **315**, 966 (2007).

[96] T. Lund-Hansen, S. Stobbe, B. Julsgaard, H. Thyrrestrup, T. Sünner, M. Kamp, A. Forchel, and P. Lodahl, Experimental Realization of Highly Efficient Broadband Coupling of Single Quantum Dots to a Photonic Crystal Waveguide, Phys. Rev. Lett. **101**, 113903 (2008).

[97] J. Gao, F. W. Sun, and C. W. Wong, Implementation scheme for quantum controlled phase-flip gate through quantum dot in slow-light photonic crystal waveguide, Appl. Phys. Lett. **93**, 151108 (2008).

[98] D. Press, K. D. Greve, P. L. McMahon, T. D. Ladd, B. Friess, C. Schneider, M. Kamp, S. Höfling, A. Forchel, and Y. Yamamoto, Ultrafast optical spin echo in a single quantum dot, Nat. Photon. **4**, 367 (2010).

[99] D. J. Reilly, J. M. Taylor, J. R. Petta, C. M. Marcus, M. P. Hanson, and A. C. Gossard, Suppressing spin qubit dephasing by nuclear state preparation, Science **321**, 817 (2008).

[100] E. Waks, E. Diamanti, and Y. Yamamoto, Generation of photon number states, New J. Phys. **8**, 4 (2006).

[101] A. B. U'Ren, C. Silberhorn, K. Banaszek, and I. A. Walmsley, Efficient Conditional Preparation of High-Fidelity Single Photon States for Fiber-Optic Quantum Networks, Phys. Rev. Lett. **93**, 093601 (2004).

[102] P. Kolchin, N. Pholchai, M. H. Mikkelsen, J. Oh, S. Ota, M. S. Islam, X. B. Yin, and X. Zhang, High purcell factor due to coupling of a single emitter to a dielectric slot waveguide, Nano Lett. **15**, 464 (2015).

[103] F. B. Basset, S. Bietti, A. Tuktamyshev, S. Vichi, E. Bonera, and S. Sanguinetti, Spectral broadening in self-assembled GaAs quantum dots with narrow size distribution, J. Appl. Phys. **126**, 024301 (2019).

[104] A. Mittelstädt, L. A. Th. Greif, S. T. Jagsch, and A. Schliwa, Terahertz lasing at room temperature: A numerical study of a vertical-emitting quantum cascade laser based on a quantum dot superlattice, Phys. Rev. B **103**, 115301 (2021).